AGU PUBLICATIONS

Geophysical Research Letters

RESEARCH LETTER
10.1002/2016GL068051

Key Points:
- We test the importance of mixed layer eddies to phytoplankton blooms using a Lagrangian approach
- Mixed layer eddies can advance the timing of the bloom by 1 to 2 weeks
- Blooms are tightly linked to heat fluxes, whether or not mixed layer eddies are present

Supporting Information:
- Supporting Information S1

Correspondence to:
S. R. Brody,
sarah_brody@mckinsey.com

Citation:
Brody, S. R., M. S. Lozier, and A. Mahadevan (2016), Quantifying the impact of submesoscale processes on the spring phytoplankton bloom in a turbulent upper ocean using a Lagrangian approach, *Geophys. Res. Lett.*, *43*, 5160–5169, doi:10.1002/2016GL068051.

Received 7 DEC 2015
Accepted 15 APR 2016
Accepted article online 30 APR 2016
Published online 18 MAY 2016

Quantifying the impact of submesoscale processes on the spring phytoplankton bloom in a turbulent upper ocean using a Lagrangian approach

Sarah R. Brody[1,2], M. Susan Lozier[1], and Amala Mahadevan[3]

[1]Division of Earth and Ocean Sciences, Duke University, Durham, North Carolina, USA, [2]Now at McKinsey & Company, Washington, District of Columbia, USA, [3]Department of Physical Oceanography, Woods Hole Oceanographic Institution, Woods Hole, Massachusetts, USA

Abstract The spring phytoplankton bloom in the subpolar North Atlantic and the mechanisms controlling its evolution and onset have important consequences for marine ecosystems and carbon cycling. Submesoscale mixed layer eddies (MLEs) play a role in the onset of the bloom by creating localized stratification and alleviating phytoplankton light limitation; however, the importance of MLEs for phytoplankton in a turbulent surface mixed layer has not yet been examined. We explore the effect of MLEs on phytoplankton by simulating their trajectories with Lagrangian particles subject to turbulent vertical displacements in an MLE-resolving model. By tracking the light exposure of the simulated phytoplankton, we find that MLEs can advance the timing of the spring bloom by 1 to 2 weeks, depending on surface forcing conditions. The onset of the bloom is linked with the onset of positive heat fluxes, whether or not MLEs are present.

1. Introduction

In the subpolar North Atlantic Ocean, the annual spring phytoplankton bloom is a dramatic event that is visible from space [*Behrenfeld*, 2010] and is important for the marine carbon cycle [*Sabine et al.*, 2004; *Lutz et al.*, 2007] and ecosystem [*Koeller et al.*, 2009; *Edwards and Richardson*, 2004]. The prominence of the North Atlantic spring bloom has elicited numerous investigations and multiple theories to explain its timing. Most of these theories assume light to be the primary factor limiting subpolar phytoplankton growth, although grazing rates have also been proposed [*Behrenfeld*, 2010; *Boss and Behrenfeld*, 2010; *Behrenfeld et al.*, 2013]. Broadly, the light limitation-based theories can be divided based on whether they invoke one-dimensional or three-dimensional ocean physics as a control on the initiation of the bloom.

One-dimensional theories were first advanced with the Sverdrup hypothesis [*Sverdrup*, 1953], which states that subpolar phytoplankton blooms begin when ocean warming causes the mixed layer to shoal in the spring, increasing phytoplankton light availability. Recent studies have expanded upon the Sverdrup hypothesis by proposing that phytoplankton growth can occur even when mixed layers are deep provided that turbulence within the upper ocean decreases [*Huisman et al.*, 1999], due to the onset of positive heat fluxes and shutdown of turbulent convection [*Taylor and Ferrari*, 2011a; *Ferrari et al.*, 2014] or a decrease in winds [*Chiswell*, 2011]. Observations have also shown that blooms can begin while the ocean surface is still cooling; i.e., heat fluxes are negative [*Brody and Lozier*, 2014; *Mahadevan et al.*, 2012]. A shift from buoyancy-driven to wind-driven mixing, facilitated by the weakening of surface cooling, has been proposed as a one-dimensional mechanism by which blooms can begin prior to the onset of positive heat fluxes (i.e., ocean surface warming) [*Brody and Lozier*, 2014, 2015].

In contrast, other studies have highlighted the potential importance of three-dimensional ocean physics in initiating the spring bloom [*Lévy et al.*, 1998, 1999; *Taylor and Ferrari*, 2011b; *Olita et al.*, 2014; *Mahadevan et al.*, 2012]. In the subpolar North Atlantic, *Mahadevan et al.* [2012] examined the impact of meridional surface temperature gradients on the spring phytoplankton bloom south of Iceland. These gradients form density fronts within the ocean mixed layer, with warmer, lighter water to the south of the front. The fronts, maintained by the Coriolis force, create a reservoir of potential energy [*Tandon and Garrett*, 1994]. Mixed layer instabilities

can tap into this potential energy to produce mixed layer eddies (MLEs) [*Boccaletti et al.*, 2007; *Fox-Kemper et al.*, 2008]. Under favorable wind conditions and weakening negative heat fluxes, the MLEs cause the fronts to slump, creating localized stratification that traps phytoplankton within the upper ocean, allowing a bloom to begin [*Mahadevan et al.*, 2012].

Both a decrease in turbulence due to the shift from buoyancy to wind-driven mixing and localized stratification due to MLEs can explain the initiation of blooms prior to the onset of positive heat fluxes. However, current observations are insufficient to determine the relative importance of these mechanisms to the timing of the spring bloom. Indeed, the same observations were used as evidence for the weakening of negative heat fluxes [*Brody and Lozier*, 2015] and as evidence for MLEs as the primary driver of the spring bloom [*Mahadevan et al.*, 2012]. While modeling work supporting the role of MLEs in prompting the spring bloom has been conducted [*Mahadevan et al.*, 2012], that study did not take into account the light exposure phytoplankton receive as they traverse a turbulent surface mixed layer; nor did it account for how stratification can modify these turbulent pathways.

The degree to which phytoplankton light limitation is alleviated by MLEs rather than seasonal changes in wind or buoyancy forcing has important consequences for the spatial and temporal variability of the subpolar spring bloom in the North Atlantic. If seasonal heat fluxes dominate the bloom signal, a more spatially coherent response to large-scale dynamics like the North Atlantic Oscillation [*Henson et al.*, 2009] or climate change [*Henson et al.*, 2010, 2013] might be expected. Additionally, the importance of eddy-induced stratification as a control on subpolar phytoplankton blooms has implications for the ability of global climate and Earth system models to resolve bloom dynamics [*Fox-Kemper et al.*, 2008] and carbon export during bloom events [*Omand et al.*, 2015].

In this study, we quantify the effect of MLEs on the timing of the spring bloom from the perspective of phytoplankton in a turbulent upper ocean using a process study model that can resolve MLEs. The model is seeded with Lagrangian particles whose trajectories are simulated using an algorithm based on an observed turbulent flow field. We compare the light history of these particles with and without MLEs under different heat flux scenarios to examine the effect of MLEs on the spring bloom.

2. Methods

We model the Lagrangian motion of particles in the upper ocean using the nonhydrostatic Process Study Ocean Model (PSOM) [*Mahadevan et al.*, 1996; *Mahadevan*, 2006], used to investigate subpolar spring phytoplankton bloom dynamics in *Mahadevan et al.* [2012], and a scheme to displace the particles according to the estimated strength of turbulence. We perform six model runs by varying the model initial density conditions, buoyancy forcing, and wind forcing.

2.1. Model Setup

As in *Mahadevan et al.* [2012], the PSOM domain is 96 km in the x (east-west) direction, 480 km in the y (north-south) direction, and 1000 m in the z direction, with a horizontal resolution of 1 km, a stretched vertical grid with a resolution of 5 m at the surface of the domain and 50 m at the bottom, and a time step of 432 seconds. We seed the model with 100 particles. The particles are distributed evenly in the vertical and on the southwest-northeast diagonal. At each time step, we linearly interpolate the model buoyancy frequency and velocity fields to the particle positions, basing velocities on the nondivergent volume fluxes at grid cell faces of the model. We then integrate the particle velocities using a trapezoidal time-stepping scheme to move the particles forward. We then simulate the effect of turbulence on the particles by adding a turbulent vertical displacement (see section 2.4). To match the model boundary conditions, we use periodic boundary conditions for particles in the x direction and absorbing boundary conditions in the y direction. We use reflective boundary condition in the z direction (section 2.4). We seed one of the six model runs with 500 particles, in order to test the sensitivity of our results to the number of particles.

2.2. Model Initial Conditions

We initialize the model density field with lateral gradients to create MLEs and without density gradients to create no-MLE control runs. We refer to these scenarios as the MLE and no-MLE cases. As in *Mahadevan et al.* [2012], for the MLE scenario, the model is initialized with three density fronts in the east-west direction, with a density difference of 0.02 kg m^{-3} across each front, extending to the mixed layer depth, below which the domain is stratified (Figure 1a). Surface density evolves in the model until, after ~50 days, the horizontal

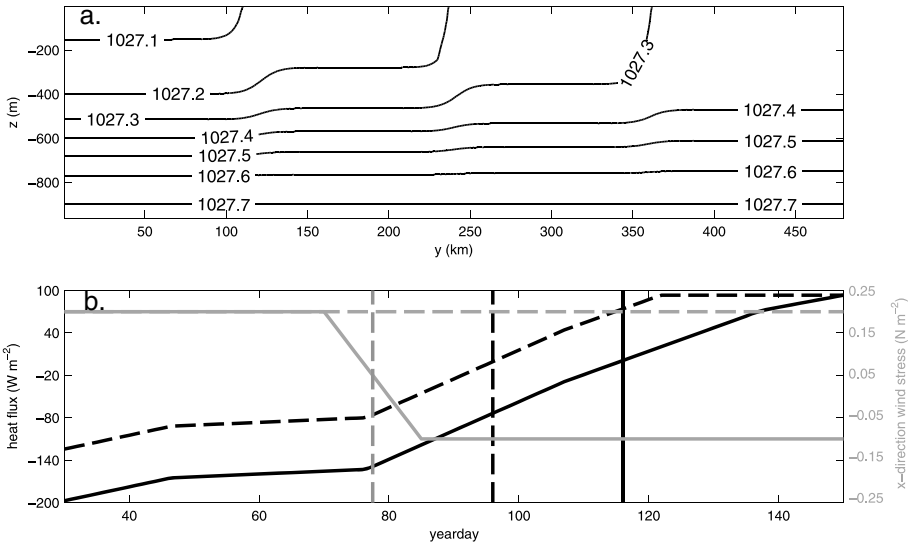

Figure 1. (a) Model initial density configuration for MLE scenario. (b) Model wind (grey lines) and heat flux (black lines) boundary conditions for both heat flux and wind scenarios. Black vertical lines indicate the yearday in which heat fluxes become positive for both scenarios, and grey vertical line indicates when winds become favorably directed for MLE formation in the original wind scenario.

density field resembles observations during the North Atlantic Bloom 2008 (NAB08) experiment [*Mahadevan et al.*, 2012]. In this model run, heat fluxes decrease linearly from north to south in order to maintain a lateral density gradient. In the no-MLE scenario, density is horizontally uniform and there is no lateral density gradient in heat fluxes. In both the MLE and no-MLE scenarios, the initial density is weakly stratified to the mixed layer depth and more strongly stratified below.

2.3. Model Boundary Conditions

The model surface is forced by heat fluxes and wind stress. We create two heat flux scenarios. In one scenario, heat fluxes are idealized versions of the atmospheric conditions during February–May 2008, the time period of the NAB08 experiment, as in *Mahadevan et al.* [2012]. Heat fluxes (Q) are strongly negative (flux out of the ocean) at the beginning of the model run and become positive on yearday 116 (the heat flux zero crossing or ZC, Figure 1b). In the second scenario, we add 73 W m^{-2} to advance the date of the heat flux zero crossing by 20 days (Figure 1b), consistent with typical year-to-year variability in the ZC (supporting information Text S1.1). We refer to these heat flux scenarios as the early-ZC and late-ZC cases, both of which are run under MLE and no-MLE conditions.

Wind stress, τ, is in the x direction only and is 0.2 N m^{-2} in the easterly direction (down-front, countering restratification) until yearday 70, after which winds linearly decrease and change direction, becoming 0.1 N m^{-2} in the westerly direction (up-front, favorable to restratification) until the end of the model run at yearday 150 (Figure 1b). Winds are tapered to zero within the northernmost and southernmost 48 km of the domain. We create two additional scenarios using the late-ZC heat fluxes: wind stress is held constant in the down-front x direction at 0.2 N m^{-2} for the MLE and no-MLE initializations. We refer to these as the constant wind scenarios to contrast with the original wind scenarios, described above. Thus, we create and compare six model runs.

2.4. Turbulence

In PSOM, we parameterize vertical mixing with a diffusivity profile dependent on wind forcing, as in *Mahadevan et al.* [2012]. Convective adjustment is turned on to prevent unstable density profiles in the presence of strong convection. While this results in well-mixed density profiles during these time periods, the model's vertical velocities do not reflect this turbulence. To account for it, we move the Langrangian particles vertically within the model domain based upon the estimated strength of turbulence at the particle position. We determine the size of these vertical displacements using a data-based approach.

Specifically, we calculate the size of the displacements using information from the trajectories of autonomous Lagrangian floats, which are designed to be neutrally buoyant [*D'Asaro et al.*, 1996; *D'Asaro*, 2008] and can

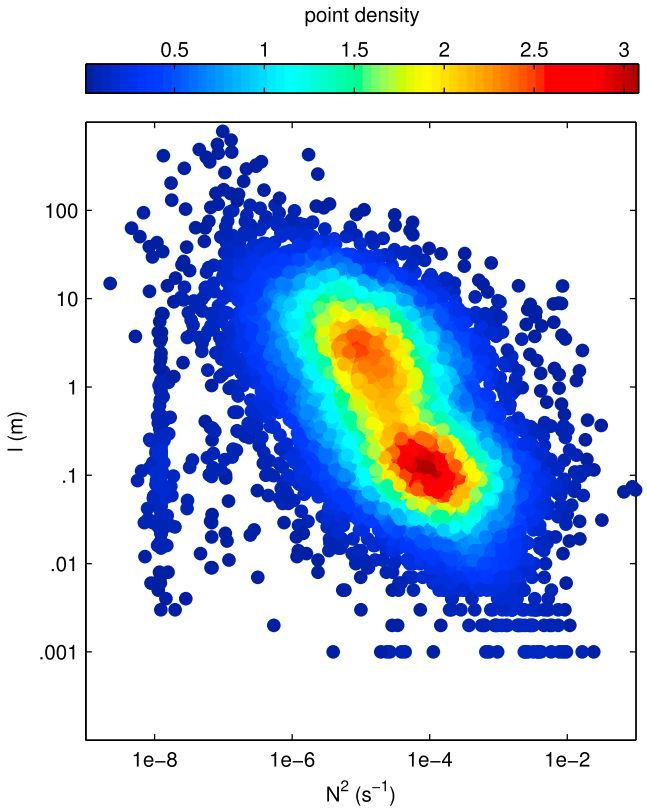

Figure 2. Magnitude of turbulent vertical motions (*l*) plotted versus the mean N^2 at the location of each *l* from data collected during the NAB08 and Lab Sea experiments, plotted on a log-log scale.

therefore follow the three-dimensional flow field. The floats were released during periods of strong convection (Labrador Sea Deep Convection Experiment [*Krahmann et al.*, 2003]) and during periods of strong wind-driven mixing (the NAB08 experiment [*Fennel et al.*, 2011]) in the subpolar North Atlantic. Details of the float programs can be found in *Steffen and D'Asaro* [2002], *Davis et al.* [1992], *Lavender et al.* [2000], *Briggs et al.* [2011], and *Cetinic et al.* [2012]. We acknowledge that Lagrangian floats differ in mass and size from phytoplankton, yet we assume that their vertical motions are similar in the upper ocean, since here water velocities are much larger than either phytoplankton sinking velocities or any biases in float motion [*D'Asaro*, 2008]. We calculate the length of the floats' coherent vertical motions, i.e., the vertical distances the floats travel before changing directions (*l*), and the average buoyancy frequency (N^2) over each *l*. The floats' displacement *l* displays a strong negative relationship to the observed buoyancy frequency (Figure 2), likely because larger turbulent vertical motions are associated with lower stratification. Using this relationship between *l* and N^2, we calculate a vertical displacement for each particle based on its N^2 value. Similarly, we calculate a time scale (Δt_l) for each particle. *l* and Δt_l are drawn randomly from a distribution and then used to vertically and temporally displace the particle. See supporting information Text S1.2 for additional details and supporting information Text S1.3 for a validation of this data-based approach. We additionally calculated displacements based on turbulent diffusivity values [*Ross and Sharples*, 2004] but found that our data-based approach better approximates the seasonal shift from deep convective mixing to shallow, wind-driven mixing (supporting information Text S1.4).

We note that while our method of adding turbulent displacements to the particles approximates well the behavior of Lagrangian floats under a variety of mixing regimes (Figures S5 and S6), the use of local N^2 to determine the displacements means that particles can easily enter and aggregate in regions of high N^2 from which the particles are less likely to escape, a potential disadvantage to this method.

2.5. Particle Light History and Bloom Initiation

We calculate irradiance along the particle trajectories using the exponential decay of light with depth $I(z) = I_o e^{-Kz}$, where I_o is the surface photosynthetically available radiation (PAR) and *K* is the light attenuation coefficient. We extract 8 day, 9 km *K* and PAR values from MODIS satellite data for a 4° latitude by 8°

longitude box surrounding the location of the NAB08 experiment during February through May 2008 using the NASA Giovanni data server (http://disc.sci.gsfc.nasa.gov/giovanni). We average within the box and interpolate in time to create time series of K and PAR that match the model time period.

Because we are estimating the bloom from individual particles, we calculate the bloom initiation date for each particle as the date on which the particle irradiance exceeds the compensation irradiance (I_c), the minimum light level at which phytoplankton growth can exceed respiration [*Sverdrup*, 1953], for a sustained period of time. We consider a bloom to be initiated for each particle when the particle's irradiance exceeds I_c for a threshold number of hours. To test the sensitivity of our results to this calculation, we chose several thresholds, all on the order of the expected time scales for phytoplankton growth (6–24 h) [*Eppley*, 1972].

I_c is difficult to measure in a laboratory setting [*Platt et al.*, 1991; *Smetacek and Passow*, 1990; *Marra*, 2004] and varies considerably for different phytoplankton species [*Langdon*, 1987]. To estimate I_c for the subpolar North Atlantic phyoplankton community while accounting for uncertainty in this value, we use a range of I_c values, from in situ [*Marra*, 2004] and satellite [*Siegel et al.*, 2002] data. These values range from 0.063 to 1.75 mol photon $m^2 d^{-1}$. See Table S1 for the complete list of I_c values.

Additionally, we compare the bloom initiation dates calculated from particle trajectories in the MLE, and late-ZC scenario with bloom initiation dates calculated based on the average light within the mixed layer, to approximate the assumptions about phytoplankton light exposure made in *Mahadevan et al.* [2012]. We define the mixed layer using the 0.01 and 0.03 kg m^{-3} density difference criteria and calculate mixed layers using density profiles at the particle positions.

3. Results

3.1. Particle Trajectory Depths

In all cases, particles are distributed over the depth of the model domain at the beginning of the run, with some enhanced concentration at the bottom of the domain (Figures 3 and S7). We find the average depth of the particle trajectories to be relatively insensitive to the use of 500, rather than 100 particles (Figure S8). As the model runs progress, particles begin shoaling and aggregating within approximately the top 50 m of the model domain, where stratification is highest (Figures 3 and S7). In the MLE scenarios, particles gradually aggregate at the surface before the heat flux ZC (Figure 3), generally in the areas of the model domain subject to eddy-induced restratification (Figure S9). After the heat flux ZC, particles shoal more uniformly throughout the model domain (Figures 3 and S9). In the no-MLE scenarios, particles remain at depth until the onset of positive heat fluxes, at which point stratification increases and the bulk of the particles shoal to the surface of the model domain (Figure 3 and S9).

The difference in MLE and no-MLE particle trajectories becomes apparent at day ~85 in the original wind scenarios, regardless of the heat flux magnitude (Figures 3, S7a, and S7b). At this point in the model run, winds become favorable to MLE-induced stratification and cooling abates rapidly in both the early-ZC and late-ZC scenarios (Figure 1b). Both of these changes in the surface forcing play a role in generating MLEs and creating localized stratification at day ~85 (Figure 3). In the constant wind scenarios (Figures 3 and S7c) the depths of particles in the MLE and no-MLE cases remain similar until day ~95, again indicating the role of favorable winds in contributing to localized stratification induced by MLEs. The magnitude of heat fluxes and timing of the heat flux ZC influences the shoaling of the particle trajectories as well: although particles in both MLE original wind scenarios begin to shoal at day ~85, the early-ZC MLE particles (red line in Figure S7b, and Figure 3, third panel) shoal more rapidly than the late-ZC MLE particles (red line in Figure S7a, and Figure 3, first panel).

3.2. Bloom Initiation Dates

We find consistent ranges in bloom initiation dates across I_c values and consistent differences between MLE/no-MLE and early/late-ZC bloom initiation dates at time thresholds greater than 6 h (Figure S10) and little sensitivity to the number of particles used to calculate bloom initiation dates (Figure S11). Here we present and discuss bloom initiation dates calculated using the 12 h threshold for irradiance exceeding the compensation irradiance, the threshold for which bloom timing most closely matched observations [*Brody and Lozier*, 2015] in the MLE late-ZC scenario, where initial and boundary conditions were tuned to the North Atlantic Bloom 2008 experiment [*Mahadevan et al.*, 2012].

We show particle bloom initiation dates for each scenario as distributions and averages (Figure 4 and Table S1). The MLE scenarios produce a wider temporal spread of bloom initiation dates compared with the no-MLE

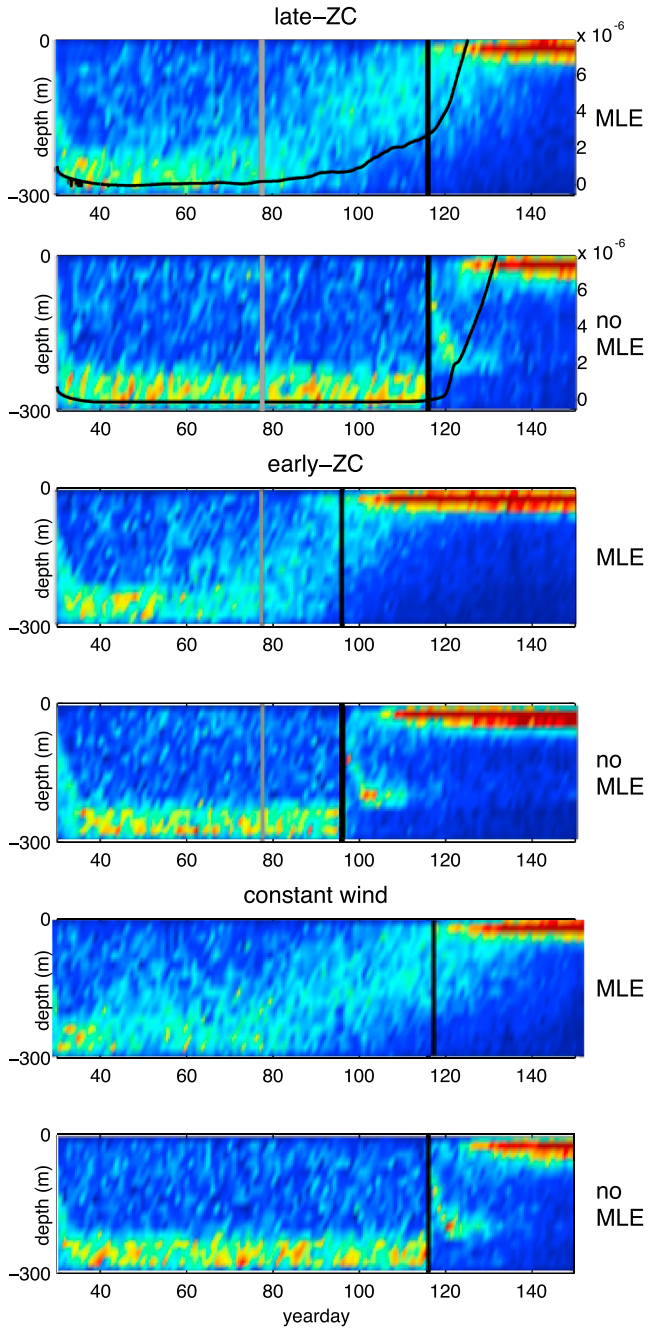

Figure 3. Depth distribution of particles in the upper 300 m of the model domain. Particle depths have been binned into 20 m, 24 h bins and normalized to the number of particles in the upper 300 m for each 24 h time period. The color axis spans 0 to 0.25. The vertical black lines indicate the heat flux zero crossings for each scenario, and the grey lines in the late-ZC and early-ZC scenarios indicate when the wind stress changes sign. The lines and right axes in the first and second panels show the average N^2 in the top 300 m of the water column at each time step for the MLE and no-MLE late-ZC scenarios.

scenarios, with the middle 50% of bloom initiation dates in the late-ZC, MLE scenario spanning 37 days, compared with 20 days for the late-ZC, no-MLE scenario. Again, this indicates a heterogeneous bloom initiation when MLEs play a role in the onset of the bloom. The distributions of MLE and no-MLE bloom initiation dates in the constant wind scenarios overlap more than the distributions in the original wind scenarios, illustrating the influence of favorable winds on early bloom initiation in the presence of MLEs. On average, MLE

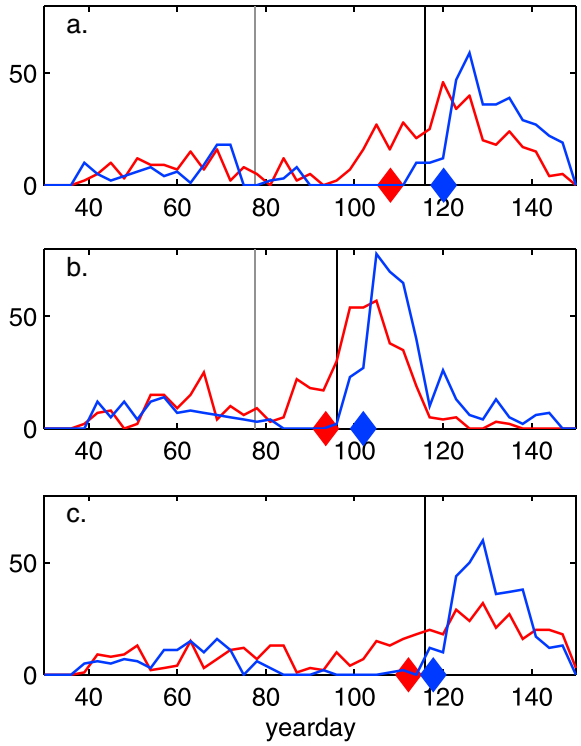

Figure 4. Distributions of bloom initiation dates using the 12 h time threshold for the MLE (red) and no-MLE (blue) particles in the (a) late-ZC, (b) early-ZC, and (c) constant wind scenarios. Distributions are created using bloom initiation dates calculated with the five I_c values for all 100 particles. Red and blue filled diamonds show the mean bloom initiation date for each distribution, and black and grey lines show the heat flux and wind zero crossings.

particles record bloom initiation dates 12 days earlier than no-MLE particles for the late-ZC, original wind scenario, compared with a difference of 6 days for the constant wind scenario.

Both late-ZC and early-ZC MLE particles record many bloom initiation dates prior to the heat flux ZCs and some instances of very early blooms (Figures 4a and 4b). These distributions lead to average bloom initiation dates that occur prior to the heat flux ZC. However, in both cases, a significant portion of bloom initiation dates occur after the heat flux ZC as well, consistent with the more uniform accumulation of particles in the upper portion of the model domain after heat fluxes become positive (Figure 3, first and third panels). This is especially true for the early-ZC distribution of bloom initiation dates. The onset of favorable winds occurs on day ~78, for both the early and late-ZC scenarios. In the early-ZC scenario, there is a shorter time window during which winds are favorable and cooling is rapid; thus, fewer particles shoal prior to the ZC. Therefore, the average bloom initiation date for early-ZC particles occurs 2 days prior to the onset of positive heat fluxes, compared with 8 days prior for late-ZC particles, and there is an 8 day, rather than 12 day, difference between MLE and no-MLE bloom initiation dates in the early-ZC scenario.

The no-MLE distributions of bloom initiation dates are even more tightly tied to the heat flux ZC than the MLE distributions. In both the early and late-ZC cases, the no-MLE particles record few instances of blooms prior to the ZC. Most bloom initiation dates occur directly after the ZC, consistent with the observed particle trajectories (Figures 3 and S7). Early and late-ZC no-MLE bloom initiation dates fall on average 6 (for early ZC) and 4 (for late ZC) days after the early and late ZCs.

We compare the bloom initiation dates calculated from the particle trajectories in the late-ZC, no-MLE scenario with those calculated using mixed layer averaged light, to estimate the effect on bloom initiation dates of adding turbulence to the particle trajectories. Bloom initiation dates calculated from particle trajectories occur later than bloom initiation dates calculated from mixed layer averaged light, especially for mixed layers calculated using a smaller density difference criteria. This is expected given that we allow the particles to escape the mixed layer and traverse the model domain.

4. Discussion

By tracking Lagrangian particles in a process study model, we are able to quantify the effect of localized stratification due to MLEs on the timing of the spring bloom. We find that MLEs cause a relatively large percentage of the bloom to occur prior to the onset of ocean surface warming and thus advance the overall timing of the spring bloom by 1 to 2 weeks relative to blooms occurring in an environment without MLEs, a time scale relevant to marine ecosystems [*Koeller et al.*, 2009]. The degree to which MLEs advance the timing of the spring bloom is sensitive to whether winds are favorably directed for MLE formation and the length of time of favorably directed winds coincide with weak ocean cooling.

We further find a tight linkage between the timing of the bloom and the date of the heat flux zero crossing in the no-MLE scenarios, and to a lesser extent in the MLE scenarios, suggesting a dominant role for heat fluxes in controlling the timing of the spring bloom, whether or not MLEs are present. This finding is consistent with previous work linking the initiation of the subpolar North Atlantic phytoplankton bloom to the onset of positive heat fluxes [*Ferrari et al.*, 2014] or weakening of negative heat fluxes [*Brody and Lozier*, 2014]. While we tested the effect of typical year-to-year heat flux variability on bloom initiation, anomalous ZCs or long-term changes in the timing of the ZC [*Yu and Weller*, 2007] may create a greater change in the timing of the spring bloom than we observe here.

While our findings suggest a significant role for MLEs and the heat flux zero crossing in setting the timing of the spring bloom, other factors we did not explicitly consider here may also play a role in controlling spring bloom initiation. From a physical perspective, our work used stratification alone to set the strength of turbulent displacements, resulting in blooms beginning on average 4–6 days after the heat flux ZC in the no-MLE scenarios, as overall stratification increases. However, mixing can abate prior to increases in stratification as cooling weakens [*Brody and Lozier*, 2014] or within hours of the heat flux ZC, as turbulent convection ceases [*Taylor and Ferrari*, 2011a]. Because we did not account for these factors, the overall timing of the spring bloom we find here may be delayed relative to the heat flux ZC, especially in the no-MLE scenarios. Further, in our idealized model setup, ocean surface warming increased consistently throughout the model runs, resulting in one heat flux ZC, whereas in reality, heat fluxes can switch signs multiple times as they become positive [e.g., *Ferrari et al.*, 2014; *Brody and Lozier*, 2015]. This heat flux variability would add some uncertainty to the bloom initiation dates, potentially causing more overlap between the MLE and no-MLE blooms.

From a biological perspective, we find a range of bloom initiation dates using different irradiance and time thresholds to define the bloom, suggesting that the light requirements of the phytoplankton community may play a role in setting the timing of the bloom [*Barton et al.*, 2015]. Additionally, we did not account for phytoplankton growth or grazing in our model setup. Seasonal decoupling of phytoplankton growth and grazing has been shown to play a role in spring bloom initiation and could arguably be the main factor controlling bloom initiation [*Behrenfeld*, 2010; *Boss and Behrenfeld*, 2010; *Behrenfeld et al.*, 2013]. Blooms driven by the decoupling of growth and grazing would occur prior to blooms driven by the alleviation of light limitation, because the decoupling occurs during the winter, when grazer populations crash due to the low concentration of phytoplankton in the water column [*Behrenfeld*, 2010]. Thus, accounting for this mechanism would potentially prompt a bloom before the onset of either MLE-driven or heat flux-drive stratification, rendering the differences between the MLE and no-MLE scenarios small by comparison. However, it is also possible that including growth and grazing in our analysis would highlight the early blooms caused by MLE-induced stratification, as the relatively few particles that shoal in locally stratified regions would not result in concentrations large enough to prompt increases in grazer populations and could therefore grow unchecked.

Because our results imply an ecologically significant role for mixed layer eddies in controlling the timing of the bloom, this might be an important area of development for global ecosystem or Earth system models. Future work could confirm and expand on our findings using observations. The degree to which mixed layer eddies advance the timing of the spring bloom under ideal conditions suggests that this mechanism might be apparent in blooms observed using 8 day satellite chlorophyll data [*Siegel et al.*, 2002; *Henson et al.*, 2009; *Brody et al.*, 2013; *Brody and Lozier*, 2014]. Work done to gauge the importance of MLEs globally [*Fox-Kemper et al.*, 2008; *Omand et al.*, 2015] combined with analyses of bloom processes in global, depth-resolved biophysical observations [*Xing et al.*, 2011; *Brody*, 2015], can help determine observationally whether and when MLEs affect the timing of the spring phytoplankton bloom.

Acknowledgments
The authors acknowledge J. Wang for the particle trajectory code; S. Mukherjee, S. Ramachandran, and M. Claret for assistance with the PSOM-GOTM coupling; and Z. Johnson for helpful discussion related to the bloom initiation metric. This work was supported by a NASA Earth and Space Science Fellowship, by NASA grant 343-0325, and by NSF grand OCE-1434788. For further information and data, contact S. Brody.

References

Barton, A., M. Lozier, and R. Williams (2015), Physical controls of variability in North Atlantic phytoplankton communities, *Limnol. Oceanogr.*, *60*, 181–197, doi:10.1002/lno.10011.
Behrenfeld, M. (2010), Abandoning Sverdrup's critical depth hypothesis on phytoplankton blooms, *Ecology*, *91*, 977–989, doi:10.1890/09-1207.1.
Behrenfeld, M., S. Doney, I. Lima, E. Boss, and D. Siegel (2013), Annual cycles of ecological disturbance and recovery underlying the subarctic Atlantic spring plankton blooms, *Global Biogeochem. Cycles*, *27*, 526–540, doi:10.1002/gbc.20050.
Boccaletti, G., R. Ferrari, and B. Fox-Kemper (2007), Mixed layer instabilities and restratification, *J. Phys. Oceanogr.*, *37*, 2228–2250.
Boss, E., and M. Behrenfeld (2010), In situ evaluation of the initiation of the North Atlantic phytoplankton bloom, *Geophys. Res. Lett.*, *37*, L18603, doi:10.1029/2010GL044174.
Briggs, N., M. Perry, I. Cetinic, C. Lee, E. D'Asaro, A. Gray, and E. Rehm (2011), High-resolution observations of aggregate flux during a sub-polar North Atlantic spring bloom, *Deep Sea Res., Part I*, *58*, 1031–1039, doi:10.1016/j.dsr.2011.07.007.
Brody, S. (2015), Physical drivers of the spring phytoplankton bloom in the subpolar North Atlantic ocean, PhD thesis, Duke University, Ann Arbor, Mich.
Brody, S., and M. Lozier (2014), Changes in dominant mixing length scale as a driver of phytoplankton bloom initiation in the North Atlantic, *Geophys. Res. Lett.*, *41*, 3197–3203, doi:10.1002/2014GL059707.
Brody, S., and M. Lozier (2015), Characterizing upper-ocean mixing and its effect on the spring phytoplankton bloom with in situ data, *ICES J. Mar. Sci.*, *72*(6), 1961–1970, doi:10.1093/icesjms/fsv006.
Brody, S., M. Lozier, and J. Dunne (2013), A comparison of methods to determine phytoplankton bloom initiation, *J. Geophys. Res. Oceans*, *118*, 2345–2357, doi:10.1002/jgrc.20167.
Cetinic, I., M. Perry, N. Briggs, E. Kallin, E. D'Asaro, and C. Lee (2012), Particulate organic carbon and inherent optical properties during 2008 North Atlantic Bloom Experiment, *J. Geophys. Res.*, *117*, C06028, doi:10.1029/2011JC007771.
Chiswell, S. (2011), Annual cycles and spring blooms in phytoplankton: Don't abandon Sverdrup completely, *Mar. Ecol. Prog. Ser.*, *443*, 39–50, doi:10.3354/meps09453.
D'Asaro, E. (2008), Convection and seeding of the North Atlantic bloom, *J. Mar. Syst.*, *69*, 233–237, doi:10.1016/j.jmarsys.2005.08.005.
D'Asaro, E., D. Farmer, J. Osse, and G. Dairiki (1996), A Lagrangian float, *J. Atmos. Oceanic Technol.*, *13*, 1230–1246.
Davis, R., L. Regier, J. Dufour, and D. Webb (1992), The autonomous Lagrangian circulation explorer (ALACE), *J. Atmos. Oceanic Technol.*, *9*, 264–285, doi:10.1175/1520-0426(1992)009.
Edwards, M., and J. Richardson (2004), Impact of climate change on marine pelagic phenology and trophic mismatch, *Nature*, *430*, 881–884, doi:10.1038/nature02808.
Eppley, R. (1972), Temperature and phytoplankton growth in the sea, *Fish. Bull.*, *70*(4), 1063–1086.
Fennel, L., I. Cetinic, E. D'Asaro, C. Lee, and M. Perry (2011), Autonomous data describe North Atlantic spring bloom, *Eos Trans. AGU*, *92*, 465–466, doi:10.1029/2011EO500002.
Ferrari, R., S. Merrifield, and J. Taylor (2014), Shutdown of convection triggers increase of surface chlorophyll, *J. Mar. Syst.*, *147*, 116–122, doi:10.1016/j.jmarsys.2014.02.009.
Fox-Kemper, B., R. Ferrari, and R. Hallberg (2008), Parameterization of mixed layer eddies. Part I: Theory and diagnosis, *J. Phys. Oceanogr.*, *38*, 1145–1165, doi:10.1175/2007JPO3792.1.
Henson, S., J. Dunne, and J. Sarmiento (2009), Decadal variability in North Atlantic phytoplankton blooms, *J. Geophys. Res.*, *114*, C04013, doi:10.1029/2008JC005139.
Henson, S., J. Sarmiento, J. Dunne, L. Bopp, I. Lima, S. Doney, J. John, and C. Beaulieu (2010), Detection of anthropogenic climate change in satellite records of ocean chlorophyll and productivity, *Biogeosciences*, *7*, 621–640.
Henson, S., H. Cole, C. Beaulieu, and A. Yool (2013), The impact of global warming on seasonality of ocean primary production, *Biogeosciences*, *10*, 4357–4369, doi:10.5194/bg-10-4357-2013.
Huisman, J., P. van Oostveen, and F. Weissing (1999), Critical depth and critical turbulence: Two different mechanisms for the development of phytoplankton blooms, *Limnol. Oceanogr.*, *44*, 1781–1787.
Koeller, P., et al. (2009), Basin-scale coherence in phenology of shrimps and phytoplankton in the North Atlantic Ocean, *Science*, *324*(5928), 791–793, doi:10.1126/science.1170987.
Krahmann, G., et al. (2003), The Labrador Sea deep convection experiment data collection, *Geochem. Geophys. Geosyst.*, *4*, 1091, doi:10.1029/2003GC000536.
Langdon, C. (1987), On the causes of interspecific differences in the growth-irradiance relationship for phytoplankton. Part 1. A comparative study of the growth-irradiance relationship of three marine phytoplankton species: Skeletonema costatum, Olisthodiscus luteus and Gonyaulax tamarensis, *J. Plankton Res.*, *9*, 459–482.
Lavender, K., R. Davis, and W. Owens (2000), Mid-depth recirculation observed in the interior Labrador and Irminger Seas by direct velocity measurements, *Nature*, *407*, 66–69, doi:10.1038/35024048.
Lévy, M., L. Mémery, and G. Madec (1998), The onset of a bloom after deep winter convection in the northwestern Mediterranean Sea: Mesoscale process study with a primitive equation model, *J. Mar. Syst.*, *16*, 7–21.
Lévy, M., L. Mémery, and G. Madec (1999), The onset of the spring bloom in the MEDOC area: Mesoscale spatial variability, *Deep Sea Res., Part I*, *46*, 1137–1160.
Lutz, M., K. Caldeira, R. Dunbar, and M. Behrenfeld (2007), Seasonal rhythms of net primary production and particulate organic flux to depth describe the efficiency of biological pump in the global ocean, *J. Geophys. Res.*, *112*, C10011, doi:10.1029/2006JC003706.
Mahadevan, A. (2006), Modeling vertical motion at ocean fronts: Are nonhydrostatic effects relevant at submesoscales?, *Ocean Model.*, *14*, 222–240.
Mahadevan, A., J. Oliger, and R. Street (1996), A nonhydrostatic mesoscale ocean model. Part II: Numerical complementation, *J. Phys. Oceanogr.*, *26*, 1881–1900, doi:10.1175/1520-0485.
Mahadevan, A., E. D'Asaro, C. Lee, and M. Perry (2012), Eddy-driven stratification initiates North Atlantic spring phytoplankton blooms, *Science*, *337*, 54–58, doi:10.1126/science.1218740.
Marra, J. (2004), The compensation irradiance for phytoplankton in nature, *Geophys. Res. Lett.*, *31*, L06305, doi:10.1029/2003GL018881.
Olita, A., S. Sparnocchia, S. Cusi, L. Fazioli, R. Sorgente, J. Tintoré, and A. Ribotti (2014), Observations of a phytoplankton spring bloom onset triggered by a density front in NW Mediterranean, *Ocean Sci.*, *10*, 657–666, doi:10.5194/os-10-657-2014.
Omand, M., E. D'Asaro, C. Lee, M.-J. Perry, N. Briggs, I. Cetinic, and A. Mahadevan (2015), Eddy-driven subduction exports particulate carbon from the spring bloom, *Science*, *348*, 222–225, doi:10.1126/science.1260062.
Platt, T., D. Bird, and S. Sathyendranath (1991), Critcal depth and marine primary production, *Proc. R. Soc. B*, *246*, 205–217, doi:10.1098/rspb.1991.0146.

Ross, O., and J. Sharples (2004), Recipe for 1-D Lagrangian particle tracking models in space-varying diffusivity, *Limnol. Oceanogr. Methods*, *2*, 289–302, doi:10.4319/lom.2004.2.289.

Sabine, C., et al. (2004), The oceanic sink for anthropogenic CO_2, *Science*, *305*, 367–371.

Siegel, D., S. Doney, and J. Yoder (2002), The North Atlantic spring phytoplankton bloom and Sverdrup's Critical Depth Hypothesis, *Science*, *296*(5568), 730–733, doi:10.1126/science.1069174.

Smetacek, V., and U. Passow (1990), Spring bloom initiation and Sverdrup's critical depth model, *Limnol. Oceanogr.*, *35*, 228–234.

Steffen, E., and E. D'Asaro (2002), Deep convection in the Labrador Sea as observed by Lagrangian floats, *J. Phys. Oceanogr.*, *32*, 475–492, doi:10.1175/1520-0485.

Tandon, A., and C. Garrett (1994), Mixed layer stratification due to a horizontal density gradient, *J. Phys. Oceanogr.*, *24*, 1419–1424, doi:10.1175/1520-0485.

Taylor, J., and R. Ferrari (2011a), Shutdown of turbulent convection as a new criterion for the onset of spring phytoplankton blooms, *Limnol. Oceanogr.*, *56*, 2293–2307, doi:10.4319/lo.2011.56.6.229.

Taylor, J., and R. Ferrari (2011b), Ocean fronts trigger high latitude phytoplankton blooms, *Geophys. Res. Lett.*, *38*, L23601, doi:10.1029/2011GL049312.

Sverdrup, H. (1953), On conditions for the vernal blooming of phytoplankton, *J. Conseil Int. pour L'Explor. de la Mer*, *18*, 287–295.

Xing, X., A. Morel, H. Claustre, D. Antoine, F. D'Ortenzio, A. Poteau, and A. Mignot (2011), Combined processing and mutual interpretation of radiometry and fluorometry from autonomous profiling bio-argo floats: Chlorophyll a retrieval, *J. Geophys. Res.*, *116*, C06020, doi:10.1029/2010JC006899.

Yu, L., and R. Weller (2007), Objectively analyzed air-sea heat fluxes for the global ice-free oceans (1981-2005), *Bull. Am. Meteorol. Soc.*, *88*, 527–539, doi:10.1175/BAMS-88-4-527.